Au nanoparticles deposited on the external surfaces of TS-1: Enhanced stability and activity for direct propylene epoxidation with H_2 and O_2

Xiang Feng[a], Xuezhi Duan[a], Gang Qian[a], Xinggui Zhou[a,*], De Chen[b], Weikang Yuan[a]

[a] *State Key Laboratory of Chemical Engineering, East China University of Science and Technology, 130 Meilong Road, Shanghai 200237, China*

[b] *Department of Chemical Engineering, Norwegian University of Science and Technology, Trondheim 7491, Norway*

Abstract: Au/TS-1 catalysts prepared by deposition-precipitation method are very promising for direct propylene epoxidation with H_2 and O_2. However, the catalysts usually suffer from rapid deactivation. In this work, calcined TS-1 with open micropores (TS-1-O) is first used to support Au catalysts, and then the used catalysts at different time-on-streams are characterized to understand the deactivation mechanism. The micropore blocking by carbonaceous deposits is found to be responsible for the deactivation. We therefore suggest a principle of catalyst design to improve the long term stability by depositing Au nanoparticles on the external surfaces of TS-1. For this purpose, uncalcined TS-1 with blocked micropores (TS-1-B) is used to support Au catalyst. As expected, the designed catalyst is not only very stable because of the elimination of pore blocking and the more accessible active sites, but also highly active with the PO formation rate of 125 $g_{PO}\cdot h^{-1}\cdot kg_{Cat}^{-1}$ for over 30 hours.

Keywords: Propylene epoxidation, Au/TS-1 catalyst, Deactivation mechanism, Micropore blocking, Stability

*Corresponding author. Tel.: +86-21-64253509. Fax.: +86-21-64253528. E-mail address: xgzhou@ecust.edu.cn

1 Introduction

Propylene oxide (PO) as a versatile bulk chemical intermediate is widely used in the production of a variety of derivatives such as polyurethane and polyester resins. In view of the environmental and economic objectives, the direct epoxidation of propylene with molecular H_2 and O_2 for the synthesis of PO has attracted extensive interests compared to the chlorohydrin and peroxidation processes [1]. Encouraged by the finding of Au/TiO_2 catalyst with the high PO selectivity in despite of the low propylene conversion (ca. 1%) [2], great efforts have been devoted to developing active Au catalysts supported on Ti-containing materials [3-16]. Highly dispersed Au nanoparticles deposited on titanium silicate-1 (TS-1) with both the hydrophobic surfaces and the only presence of the isolated Ti (IV) sites were found to have much higher PO formation rate (116~160 $g_{PO}{\cdot}h^{-1}{\cdot}kg_{Cat}^{-1}$ at 200 ^{o}C) than those deposited on other Ti-containing supports [17, 18]. As a result, the high formation rate of PO has been achieved to be comparable to that of ethylene oxide in commercial plants [19].

Despite the significant enhancement of the activity of Au/TS-1 catalysts, they usually suffer from rapid deactivation within several hours unless with very low Au loadings or carefully pretreated supports [18, 20-22]. The aggregation of Au nanoparticles with time-on-stream proposed by Delgass et al. [9] was used to explain the deactivation. However, this interpretation was questioned by Lu et al. [23]. Instead, he explicated the deactivation by the blocking of active sites with the bidentate species and other organic fragments. However, no direct evidence was provided to relate the formation rate of the bidentate species to the deactivation rate over Au/TS-1 catalyst [17]. Thus, a better

understanding of the deactivation mechanism is highly desired.

Recently, solid grinding (SG) [21, 24] and sol-immobilization (SI) [22, 25] methods have been used to prepare the Au/TS-1 catalysts. Although they show great stability, these catalysts have a low Au catalytic efficiency because some of the Au nanoparticles are deposited far away from the active titanium sites due to the non-selective deposition of Au nanoparticles [22, 26]. Comparatively, the commonly used deposition-precipitation (DP) method is more attractive because Au nanoparticles can be selectively deposited near the active titanium sites by adjusting the pH of the solution higher than the isoelectric point of the inactive silicon sites [27, 28]. When under similar Au particle size and without adding promoters, the PO formation rate of Au/TS-1 catalyst (160 $g_{PO}{\cdot}h^{-1}{\cdot}kg_{Cat}^{-1}$) prepared by DP method is much higher than those of Au/TS-1 catalysts prepared by SG and SI methods, which are 11 and 25 $g_{PO}{\cdot}h^{-1}{\cdot}kg_{Cat}^{-1}$, respectively [21, 25]. It is expected that the Au/TS-1 catalysts prepared by DP method will show simultaneously enhanced activity and prolonged stability.

In this work, the deactivation mechanism of conventional Au/TS-1 catalysts (i.e., Au nanoparticles supported on calcined TS-1 (TS-1-O) support) prepared by DP method is studied by characterization of used catalysts. The blocking of the micropores by carbonaceous deposits is found to be responsible for the catalyst deactivation. Analysis of the deactivation mechanism leads to a new strategy of the catalyst design to improve the catalyst stability by selectively deposition of Au nanoparticles on the external surfaces of TS-1. We therefore use uncalcined TS-1 with blocked micropores as the support in the hope that all the gold nanoparticles are on the exterior surface of the

support. The so obtained catalyst (Au/TS-1-B) is evaluated and compared with Au/TS-1-O, which shows a significant improvement in the long term stability.

2 Experimental

2.1 Synthesis of Au/TS-1-B and Au/TS-1-O catalysts

TS-1 with the Si/Ti molar ratio of 100 was synthesized using the hydrothermal method developed by Khomane et al. [29]. The as-synthesized TS-1 was either directly used to support Au nanoparticles or calcined before supporting Au nanoparticles. The resulted two catalysts with blocked or open micropores were denoted as Au/TS-1-B and Au/TS-1-O, respectively.

In a typical process, 2.0 g polyoxyethylene 20-sorbitan monolaurate (Tween 20, Aldrich) was added to 28.6 mL deionized water under vigorous stirring, and then 22.6 g tetrapropylammonium hydroxide (TPAOH, 25 wt%) and 173 mmol tetraethylorthosilicate (TEOS, 95 wt%) were added into the above clear solution. Afterwards, 1.73 mmol titanium (IV) tetrabutoxide (TBOT, 99 wt%) dissolved in 20 mL isopropanol (WAKO, 99.5 wt%) was added drop-wise. The solution was placed in Teflon autoclave at 443 K for at least 18 h. The as-synthesized TS-1 with template remaining in the micropores (i.e. TS-1-B) was washed and dried overnight at room temperature and calcined at 823 K for 5 h to yield TS-1-O which had open micropores.

The same DP procedures were used to support Au nanoparticles on TS-1-B and TS-1-O supports according to the previous report [17]. 0.1g hydrogen tetrachloroaurate(III) tribydrate ($HAuCl_4 \cdot 3H_2O$, Sinopharm Chemical Reagent Co., Ltd, 99.99%) was dissolved in 50 mL deionized water, followed by the addition of 0.5 g TS-1-B or TS-1-O supports. The slurries of Au/TS-1-B and Au/TS-1-O were neutralized

to pH of 7.3 by 1 M aqueous solution of sodium hydroxide and aged at room temperature for different times, i.e. 6.2 and 9.5 hours. The catalysts were collected by centrifugation (4000 rpm for 30 min) and washed twice with deionized water, and then dried under vacuum at room temperature for 12 h. The as-obtained Au/TS-1-B and Au/TS-1-O catalysts had Au loadings of 0.12 and 0.10 wt%, respectively.

2.2 Catalyst characterization

The crystal phases of TS-1-B and TS-1-O supports were characterized by XRD (Rigaku D/Max2550VB/PC, Cu K_α radiation). The surface areas and pore volumes of the TS-1-B and TS-1-O supports were measured in a volumetric adsorption unit (Micromeritics ASAP 2020). The contents of carbonaceous deposits were obtained by thermogravimetric analysis (Perkin Elmer TGA Pyris 1). The local environments of titanium in the TS-1-B and TS-1-O supports were determined by DRUV-vis (Perkin Elmer Lambda 35) and FT-IR (Nicolet 6700). The zeta potentials of TS-1-B and TS-1-O supports were determined on a Delsa TM Nano C particle analyzer. The Au loadings of Au/TS-1-B and Au/TS-1-O catalysts were determined by AAS (ZEEnit 600). The transmission electron microscopy (TEM) images were obtained on a JEOL JSM-2100.

2.3 Catalytic testing

The Au/TS-1-B and Au/TS-1-O catalysts were tested for the gas-phase propylene epoxidation under atmospheric pressure in a quartz tubular reactor (i.d. 8 mm) using a feed containing C_3H_6, H_2, O_2 and N_2 with the flow rate of 3.5/3.5/3.5/24.5 $mL \cdot min^{-1}$ (corresponding to a space velocity of 14,000 $mL \cdot h^{-1} \cdot g_{cat}^{-1}$), where 0.15 g catalysts of 60-80 mesh size were loaded. The two catalysts were heated from room temperature to 200 ^oC at a rate of 0.5 $^oC \cdot min^{-1}$. The catalytic tests as a function of time-on-stream in

this work started after the reaction temperature reached 200 ºC. The reactants and products were analyzed by two on-line GCs (Agilent 6890), equipped with TCD (5A column and Porapak Q column) and FID (Porapak T column), respectively. The 5A (3 mm × 3 m) and Porapak Q columns (3 mm × 3 m) were used to detect hydrocarbons, H_2, O_2, N_2, CO_x and H_2O, while the Porapak T column (3 mm × 3 m) was used to detect oxygenates (e.g., propylene, propane, acetaldehyde, PO, acetone and propanal). Blank tests indicated that no PO was generated in the blank reactor.

3 Results and discussion

3.1 Deactivation behavior of Au/TS-1-O catalyst

Fig. 1 shows the PO formation rate of 0.10 wt% Au/TS-1-O catalyst with time-on-stream. The selectivity to propylene oxide is nearly constant at 90%, while the PO formation rate decreases in different rates for the first 24 hours, and then remains almost unchanged from 24 to 30 h. This unique deactivation phenomenon can be explained by different deactivation mechanisms, in which Au sintering and carbonaceous deposits formation on different catalysts sites are among the possible deactivation mechanisms [9, 17, 23]. Characterization of used catalysts at different time-on-streams (e.g., TEM, TGA and N_2 physisorption) [9, 17, 23, 30-34] is necessary to elucidate the deactivation mechanism of Au/TS-1-O catalyst during the propylene epoxidation reaction.

(Fig. 1 should be inserted here)

The average sizes of the gold nanoparticles on Au/TS-1-O catalysts used at 200 ºC

for 4 and 30 h are almost the same, as indicated by TEM images (Fig. S1). The negligible change in Au particle size was also observed by Lu et al. [23]. This excludes the aggregation of Au as the dominating deactivation mechanism. Fig. 2a shows the PO formation rate divided by the initial PO formation rate (R/R_0) as a function of the content of carbonaceous deposits. With the increase of carbonaceous deposits, the PO formation rate decreases in an exponential curve, implying that the deactivation of Au/TS-1-O catalyst is due to the formation of carbonaceous deposits. The deactivation modes of the 0.10 wt% Au/TS-1-O catalyst by the carbonaceous deposits may be the active site coverage and/or the pore blocking, which can be discriminated by an analysis of relative changes in the pore volumes and volumes of carbonaceous deposits formed [34].

(Fig. 2 should be inserted here)

When the carbonaceous deposits cover the active site, the volume occupied by carbonaceous deposits (V_c) should be equal to the volume not accessible to N_2 (V_{na}). When the carbonaceous deposits block some of the channels, V_c will be smaller than V_{na} and the difference is the empty space inaccessible to N_2 [31-33]. The closer the blocking is to the pore mouth, the larger will be the difference. V_c is determined by TGA, which is the weight of carbonaceous deposits divided by the estimated density of carbonaceous deposits, and V_{na} is determined by N_2 physisorption, which is the volume of fresh Au catalyst minus that of used Au catalyst (Table 1 and Fig. S2).

(Table 1 should be inserted here)

Fig. 2b shows the changes of V_c/V_{na} with time-on-stream for Au/TS-1-O catalyst, in

which the carbonaceous deposits density is assumed to be 1.2 $g \cdot cm^{-3}$ (Fig. S3), in agreement with the results in Ref. [33, 34]. It was obtained by repeating the experiment with fresh catalyst under the same operating condition, but at different on-stream times. The used catalyst was then unloaded for analysis. As can be seen in Fig. 2b, in the initial 13 hours, the V_c/V_{na} ratio decreased from 1.00 to 0.81, strongly indicating that the micropore blocking by the carbonaceous deposits was responsible for the deactivation of the Au/TS-1-O catalyst. When the time-on-stream was longer than 13 h, the drop of the V_c/V_{na} ratio became slower, which was possibly because that most of the micropores were blocked and some of the newly formed carbonaceous deposits were on the external surface of the support. In this situation, the carbonaceous deposits had smaller influence on the observed activity. With the further increase in the time-on-stream up to 26 h, the V_c/V_{na} ratio on the contrary slightly increased. This is because the blockage extent nearly reached a limit and thus the V_{na} remained almost constant while V_c still increased due to the carbonaceous species kept depositing on the exterior surface of the catalyst. Accompanying this phenomenon was the almost unchanged PO formation rate (Fig. 1). It indicates that even with carbonaceous deposits on the external surface, the gold particles are still active. This may be because the carbonaceous deposits are possibly formed on inactive sites for propene epoxidation, or the carbonaceous deposits formed have migrated away for the active sites for epoxidation. Nevertheless, the carbonaceous deposits inside the pores lead to deactivation by constituting addition diffusion resistance and preventing the adsorption of propene and desorption of propylene oxide. Therefore, selectively depositing Au nanoparticles on the external surfaces could be a good strategy to suppress the micropore blocking deactivation of Au/TS-1-O catalyst by carbonaceous deposits.

3.2 Au nanoparticles on the external surfaces of TS-1-B support (Au/TS-1-B catalyst)

On the basis of above conclusion that the deactivation is due to pore blocking, we turned to the possibility of supporting Au nanoparticles on the external surfaces of TS-1-O support. Traditionally, before calcination, the as synthesized TS-1 contains tetrapropylammonium ion (TPA template) (Table 2) in the micropores, with its nitrogen atom at the center of channel intersection and the propyl groups extending along the channels [35]. The TPA template is usually removed by calcination to dredge the micropores [35, 36]. If the TPA template is kept in the micropores, the gold precursor will not enter into the micropores, and the formed gold nanoparticles will mostly be on the exterior of the TS-1, as evidenced in Table 2.

(Table 2 should be inserted here)

The physico-chemical properties of TS-1-B and TS-1-O supports were then compared. Fig. 3a shows the XRD patterns of TS-1-O and TS-1-B supports, both of which exhibit typical MFI structure with high crystallinity degrees. The single diffraction peaks at ~24.5^{o} of the two samples indicated the presence of the orthorhombic symmetry [29]. With respect to the use of TS-1 in oxidation reactions, the coordination states of Ti species are also very essential. UV-vis spectroscopy was employed to investigate the Ti coordination state of TS-1-O and TS-1-B supports (Fig. 3b). The spectra were dominated by a characteristic absorption band located at ca. 210 nm, which is characteristic of tetrahedrally coordinated Ti ion that is isolated in framework. In addition, the lack of shoulder at 330 nm in the UV-vis spectra was an indication of the absence of extra-framework titanium [37]. Hence, the absence of calcination for TS-1-B support did not hinder the incorporation of isolated tetrahedrally coordinated Ti species into the framework. The FT-IR spectra (Fig. 3c) show characteristic bands at 960 and 550 cm^{-1}, which are possibly assigned to the stretching of Si-O-Ti bond in the

framework and the vibration of double five-membered ring [38], indicating the MFI structure and framework Ti species, respectively. The above results indicated that both of TS-1-O and TS-1-B supports had highly crystalline MFI structure and isolated Ti (IV) species in the framework. Thus, the TS-1-B is appropriate to support Au nanoparticles for the reaction. Fig. 4 shows the schematic diagram of Au locations of Au/TS-1-O and Au/TS-1-B catalysts prepared by DP method.

(Fig. 3 should be inserted here)

(Fig. 4 should be inserted here)

Due to the existence of the TPA template [35, 39] on TS-1-B, the two supports have different acid-base properties, which were reported to affect Au capture efficiency [20] and well indicated by the isoelectric point. The isoelectric point of TS-1-B support (i.e., 7.1) is higher than that of TS-1-O support (i.e., 2.9), as shown in Fig. 5. This results in a stronger interaction between the TS-1-B support and the negative Au anions [40] (e.g., $Au[(OH)_3Cl]^{-1}$ and $Au(OH)_4^{-1}$) and hence a higher Au loading efficiency.

(Fig. 5 should be inserted here)

It is noted that the template on the external surfaces of TS-1-B support (0.4 wt%) is easily decomposed at the reaction temperature (Fig. S4), thus excluding the influence of the external template on the activity of Au/TS-1-B during the stability tests. On the other hand, the TPA template on the internal surfaces is stable even at reaction temperature. The Au nanoparticles are impossible to grow in or migrate into the micropores. Therefore the Au nanoparticles will remain on the external surface.

Fig. 6 shows the representative TEM images of the as-prepared two Au catalysts. The

average size of observable Au nanoparticles for 0.10 wt% Au/TS-1-O and 0.12 wt% Au/TS-1-B catalysts were 3.0 and 3.2 nm, respectively.

(Fig. 6 should be inserted here)

Fig. 7 shows the PO formation rate of 0.12 wt% Au/TS-1-B catalyst as a function of time-on-stream with the PO selectivity of ca. 83%. The 0.12 wt% Au/TS-1-B catalyst was found to exhibit a significantly improved stability over the 0.10 wt% Au/TS-1-O catalyst (Fig. 1). This is because the formed PO on external active sites were easily desorbed from the external surface of the support at reaction temperature [21], inhibiting its further ring-opening or oligomerization [6, 41]. These results confirm that selectively depositing Au nanoparticles on the external surfaces of TS-1-O is indeed an effective method to obtain the highly stable Au/TS-1 catalyst for the reaction.

(Fig. 7 should be inserted here)

It is also shown in Fig. 7 that the Au/TS-1-O catalyst with Au nanoparticles deposited on both the internal and external surfaces of TS-1-O showed high initial PO formation rate of 174 $g_{PO}{\cdot}h^{-1}{\cdot}kg_{Cat}^{-1}$. However, when parts of tiny Au clusters are no longer accessible after the micropore blocking by carbonaceous deposits, the PO formation rate of Au/TS-1-O catalyst decreases from the initial 174 to 113 $g_{PO}{\cdot}h^{-1}{\cdot}kg_{Cat}^{-1}$, which is slightly lower than that of Au/TS-1-B catalyst (i.e., 125 $g_{PO}{\cdot}h^{-1}{\cdot}kg_{Cat}^{-1}$) with Au nanoparticles only deposited on the external surfaces. This can be explained by the results in Ref. [15] that parts of Au clusters deposited inside the microporous channels of TS-1-O supports are more active towards PO production.

Table 3 gives a comparison of the activities between Au/TS-1-B and other stable Au/Ti-containing catalysts taken from the literatures under the similar Au mean particle

size (ca. 3-5 nm) [21, 25] at 200 ^{o}C, in which all the catalysts were without promoters. Notably, SI, SG and DP methods are all effective methods to prepare active and stable Au/TS-1 catalysts. However, the DP method could selectively deposit Au nanoparticles close to the active titanium sites instead of the inactive silicon sites [22, 26], which could be one main reason for the higher activity of the stable Au/TS-1-B catalyst without adding promoters.

(Table 3 should be inserted here)

In addition, Haruta and co-workers reported that the Au nanoparticles prepared by DP method showed hemispherical shapes, which gives longer distance of the perimeter interface with the support and is indispensable for the epoxidation of propylene [42]. This unique structural property of the Au catalyst prepared by DP method may be another reason responsible for the higher activity of Au/TS-1-B catalyst. Moreover, the activity of Au/TS-1-B catalyst could be further enhanced by adding promoters, such as ionic liquid or NH_4NO_3 [20, 22]. Both the shape effect and promoter effect of Au/TS-1-B catalysts are interesting subjects, and will be carried out in our future study.

4 Conclusions

In summary, the severe decrease of PO formation rate in the initial hours and subsequent stable PO formation rate of the 0.10 wt% Au/TS-1-O catalyst with time-on-stream were observed, and the corresponding deactivation mechanism was investigated in detail. Results showed that pore blocking by carbonaceous species was responsible for the deactivation.

The strategy, selectively depositing Au nanoparticles on the exterior surfaces of TS-1 support, was proposed to suppress the deactivation of pore blocking. This was achieved

by using uncalcined TS-1 with blocked pores (TS-1-B) as support because the TS-1-B had not only pre-filled micropores, but also similar structural properties to calcined TS-1 with open pores (TS-1-O). The 0.12 wt% Au/TS-1-B exhibited not only as expected higher stability than the 0.10 wt% Au/TS-1-O catalyst because of the elimination of pore blocking and easily accessible active sites on the external surface of TS-1-B, but also higher PO formation rate than the reported stable Au/Ti-containing catalysts under the comparable conditions. This may be due to unique physico-chemical properties of the Au catalysts prepared by DP method (e.g., Au nanoparticles near active titanium sites and the unique microstructure). In view of the superior stability and activity, the TS-1-B support is a promising candidate for enhancing the stability and activity of Au catalysts, and the strategy of depositing metal nanoparticles on the external surfaces of the support should be also applicable to the design of other transition metal catalysts suppressing the pore blocking by carbonaceous deposits.

Acknowledgments

This work is financially supported by the Natural Science Foundation of China (U1162112), the China Postdoctoral Science Foundation (2012M520041 and 2013T60428), and the 111 Project of Ministry of Education of China (B08021).

References

[1] T.A. Nijhuis, M. Makkee, J.A. Moulijn, B.M. Weckhuysen, Ind. Eng. Chem. Res. 45 (2006) 3447-3459.
[2] T. Hayashi, K. Tanaka, M. Haruta, J. Catal. 178 (1998) 566-575.
[3] M. Haruta, B.S. Uphade, S. Tsubota, A. Miyamoto, Res. Chem. Intermed. 24 (1998) 329-336.
[4] A.K. Sinha, S. Seelan, S. Tsubota, M. Haruta, Angew. Chem. Int. Ed. 43 (2004) 1546-1548.
[5] A.K. Sinha, S. Seelan, T. Akita, S. Tsubota, M. Haruta, Appl. Catal. A 240 (2003) 243-252.
[6] B.S. Uphade, T. Akita, T. Nakamura, M. Haruta, J. Catal. 209 (2002) 331-340.
[7] G. Mul, A. Zwijnenburg, B. van der Linden, M. Makkee, J.A. Moulijn, J. Catal. 201 (2001) 128-137.
[8] Y.H. Yuan, X.G. Zhou, W. Wu, Y.R. Zhang, W.K. Yuan, L. Luo, Catal. Today 105 (2005) 544-550.
[9] N. Yap, R.P. Andres, W.N. Delgass, J. Catal. 226 (2004) 156-170.
[10] L. Xu, Y. Ren, H. Wu, Y. Liu, Z. Wang, Y. Zhang, J. Xu, H. Peng, P. Wu, J. Mater. Chem. 21 (2011)

10852-10858.
[11] Y. Ren, L. Xu, L. Zhang, J. Wang, Y. Liu, M. He, P. Wu, Pure Appl. Chem. 84 (2011) 561-578.
[12] H. Yang, D. Tang, X. Lu, Y. Yuan, J. Phys. Chem. C 113 (2009) 8186-8193.
[13] E. Sacaliuc, A.M. Beale, B.M. Weckhuysen, T.A. Nijhuis, J. Catal. 248 (2007) 235-248.
[14] J. Lu, X. Zhang, J.J. Bravo-Suárez, K.K. Bando, T. Fujitani, S.T. Oyama, J. Catal. 250 (2007) 350-359.
[15] W.-S. Lee, L.-C. Lai, M. Cem Akatay, E.A. Stach, F.H. Ribeiro, W.N. Delgass, J. Catal. 296 (2012) 31-42.
[16] G. Qian, Y.H. Yuan, W. Wu, X.G. Zhou, Stud. Surf. Sci. Catal. 159 (2006) 333-336.
[17] W.-S. Lee, M. C. Akatay, E.A. Stach, F.H. Ribeiro, W.N. Delgass, J. Catal. 287 (2012) 178-189.
[18] B. Taylor, J. Lauterbach, W.N. Delgass, Appl. Catal. A 291 (2005) 188-198.
[19] Y. Yu, J. Huang, T. Ishida, M. Haruta, in: Noritaka Mizuno (Eds.), Modern Heterogeneous Oxidation Catalysis, Wiley-VCH , Weinheim, 2009, pp. 77-124.
[20] L. Cumaranatunge, W.N. Delgass, J. Catal. 232 (2005) 38-42.
[21] J. Huang, T. Takei, T. Akita, H. Ohashi, M. Haruta, Appl. Catal. B 95 (2010) 430-438.
[22] M. Du, G. Zhan, X. Yang, H. Wang, W. Lin, Y. Zhou, J. Zhu, L. Lin, J. Huang, D. Sun, L. Jia, Q. Li, J. Catal. 283 (2011) 192-201.
[23] J. Lu, X. Zhang, J.J. Bravo-Suárez, T. Fujitani, S.T. Oyama, Catal. Today 147 (2009) 186-195.
[24] J. Huang, E. Lima, T. Akita, A. Guzmán, C. Qi, T. Takei, M. Haruta, J. Catal. 278 (2011) 8-15.
[25] G. Zhan, M. Du, D. Sun, J. Huang, X. Yang, Y. Ma, A.-R. Ibrahim, Q. Li, Ind. Eng. Chem. Res. 50 (2011) 9019-9026.
[26] T. Takei, T. Akita, I. Nakamura, T. Fujitani, M. Okumura, K. Okazaki, J. Huang, T. Ishida, M. Haruta, in: C.G. Bruce, C.J. Friederike (Eds.), Advances in Catalysis, Academic Press, Amsterdam, 2012, pp. 1-126.
[27] M. Haruta, in: B. Corain, G. Schmid, N. Toshima (Eds.), Metal Nanoclusters in Catalysis and Materials Science, Elsevier, Amsterdam, 2008, pp. 183-199.
[28] M. Haruta, B.S. Uphade, S. Tsubota, A. Miyamoto, in: S. Uemura, T. Mitsudo, T. Inui, M. Haruta (Eds.), Frontiers and Tasks of Catalysis Towards the Next Century, Proceedings of the International Symposium in Honour of Professor Tomoyuki Inui, VSP BV, Utrecht, 1998, pp. 329-339.
[29] R.B. Khomane, B.D. Kulkarni, A. Paraskar, S.R. Sainkar, Mater. Chem. Phys. 76 (2002) 99-103.
[30] D.M. Bibby, N.B. Milestone, J.E. Patterson, L.P. Aldridge, J. Catal. 97 (1986) 493-502.
[31] J.L. Sotelo, M.A. Uguina, J.L. Valverde, D.P. Serrano, Appl. Catal. A 114 (1994) 273-285.
[32] D. Chen, H.P. Rebo, K. Moljord, A. Holmen, Chem. Eng. Sci. 51 (1996) 2687-2692.
[33] A. de Lucas, P. Canizares, A. Durán, A. Carrero, Appl. Catal. A 156 (1997) 299-317.
[34] X. Zhang, Y. Wang, F. Xin, Appl. Catal. A 307 (2006) 222-230.
[35] L.M. Parker, D.M. Bibby, J.E. Patterson, Zeolites 4 (1984) 168-174.
[36] M. Milanesio, G. Artioli, A.F. Gualtieri, L. Palin, C. Lamberti, J. Am. Chem. Soc. 125 (2003) 14549-14558.
[37] E. Duprey, P. Beaunier, M.A. Springuel-Huet, F. Bozon-Verduraz, J. Fraissard, J.M. Manoli, J.M. Brégeault, J. Catal. 165 (1997) 22-32.
[38] A. Zecchina, S. Bordiga, C. Lamberti, G. Ricchiardi, D. Scarano, G. Petrini, G. Leofanti, M. Mantegazza, Catal. Today 32 (1996) 97-106.
[39] B.T. Holland, Micropor. Mesopor. Mater. 89 (2006) 291-299.
[40] F. Moreau, G.C. Bond, Catal. Today 122 (2007) 260-265.

[41] A. Ruiz, B. van der Linden, M. Makkee, G. Mul, J. Catal. 266 (2009) 286-290.
[42] M. Haruta, M. Daté, Appl. Catal. A 222 (2001) 427-437.

Table captions:

Table 1 Properties of Au/TS-1-O catalysts prepared by DP method.

Table 2 The structural properties of TS-1-B, TS-1-O and Au/TS-1-B samples.

Table 3 Catalytic activities of stable Au/Ti-containing catalysts at 200 ^{o}C.

Table 1 Properties of Au/TS-1-O catalysts prepared by DP method.

Sample[a]	w_c[b] (wt%)	V_{MP}[c] ($cm^3 \cdot g^{-1}$)	V_c[d] ($cm^3 \cdot g^{-1}$)	V_{na}[e] ($cm^3 \cdot g^{-1}$)
Au/TS-1-O-fresh	0.0	0.162	0.0000	0.000
Au/TS-1-O-*0* h	2.3	0.143	0.0191	0.019
Au/TS-1-O-*2* h	3.0	0.136	0.0250	0.026
Au/TS-1-O-*8* h	3.4	0.131	0.0283	0.031
Au/TS-1-O-*13* h	3.7	0.124	0.0308	0.038
Au/TS-1-O-*20* h	4.0	0.118	0.0333	0.044
Au/TS-1-O-*26* h	4.4	0.116	0.0367	0.046

[a] Au/TS-1-O-*n* h represents 0.10 wt% Au catalysts from the time-on-stream of n hours at 200 °C.

[b] Mass fraction of carbonaceous deposits (w_c) is determined from TGA analysis.

[c] Micropore volume (V_{MP}) is estimated by t-plot method.

[d] Volume occupied by carbonaceous deposits (V_c) = w_c/ρ_c (the estimated density of carbonaceous deposits).

[e] Volume not accessible to N_2 (V_{na}) = $V_{MP1(\text{fresh Au catalyst})} - V_{MP2\ (\text{used Au catalyst})}$.

Table 2 The structural properties of TS-1-B and TS-1-O samples.

Sample	Calcination time (h)	S_{BET} ($m^2 \cdot g^{-1}$)	V_{MP}[a] ($cm^3 \cdot g^{-1}$)	V_P[b] ($cm^3 \cdot g^{-1}$)
TS-1-O	5	517	0.23	0.26
TS-1-B	0	36	0.01	0.04
TS-1-B[c]	0	41	0.01	0.04
Au/TS-1-B	0	34	0.01	0.04
Au/TS-1-B[c]	0	42	0.01	0.04

[a] Micropore volume (V_{MP}) is estimated by t-plot method.

[b] Pore volume (V_P) is evaluated from the adsorption isotherm at the relative pressure about 0.99.

[c] The samples are treated at 200 ^oC in feed gas.

Table 3 Catalytic activities of stable Au/Ti-containing catalysts at 200 °C.

Catalyst	Preparation method	Au loading (wt%)	PO formation rate ($g_{PO} \cdot h^{-1} \cdot kg_{Cat}^{-1}$)
Au/TS-1-O [25]	SI	1.00	25 (75*)
Au/TS-1-O [21]	SG	0.10	11
Au/TS-1-B	DP	0.12	ca. 125

* The data from reaction temperature of 300 °C.

Figure captions:

Fig. 1. PO formation rate and selectivity of 0.10 wt% Au/TS-1-O catalyst as a function of time-on-stream.

Fig. 2. (a) PO formation rate divided by the initial PO formation rate (R/R_0) as a function of content of carbonaceous deposits, and (b) V_c/V_{na} of the used 0.10 wt% Au/TS-1-O catalyst at different time-on-streams. The inset in (b) shows the possible distribution of carbonaceous deposits [30].

Fig. 3. (a) XRD patterns, (b) FT-IR spectra and (c) UV-vis spectra of TS-1-B (dashed line) and TS-1-O (solid line) supports.

Fig. 4. Schematic diagram of Au locations of Au/TS-1-O and Au/TS-1-B catalysts.

Fig. 5. Zeta potentials of TS-1-B (a) and TS-1-O (b) supports versus pH values.

Fig. 6. Representative TEM images of the used (a) 0.10 wt% Au/TS-1-O and (b) 0.12 wt% Au/TS-1-B catalysts at 200 ^{o}C for 4 h. The insets show the particle size distributions of the two catalysts, and the scale bars represent 10 nm.

Fig. 7. PO formation rate of Au/TS-1-B and Au/TS-1-O catalysts as a function of the time-on-stream. The data of Au/TS-1-O catalyst as a function of the time-on-stream are taken from Fig. 1 and the inset shows the selectivity of Au/TS-1-B catalyst.

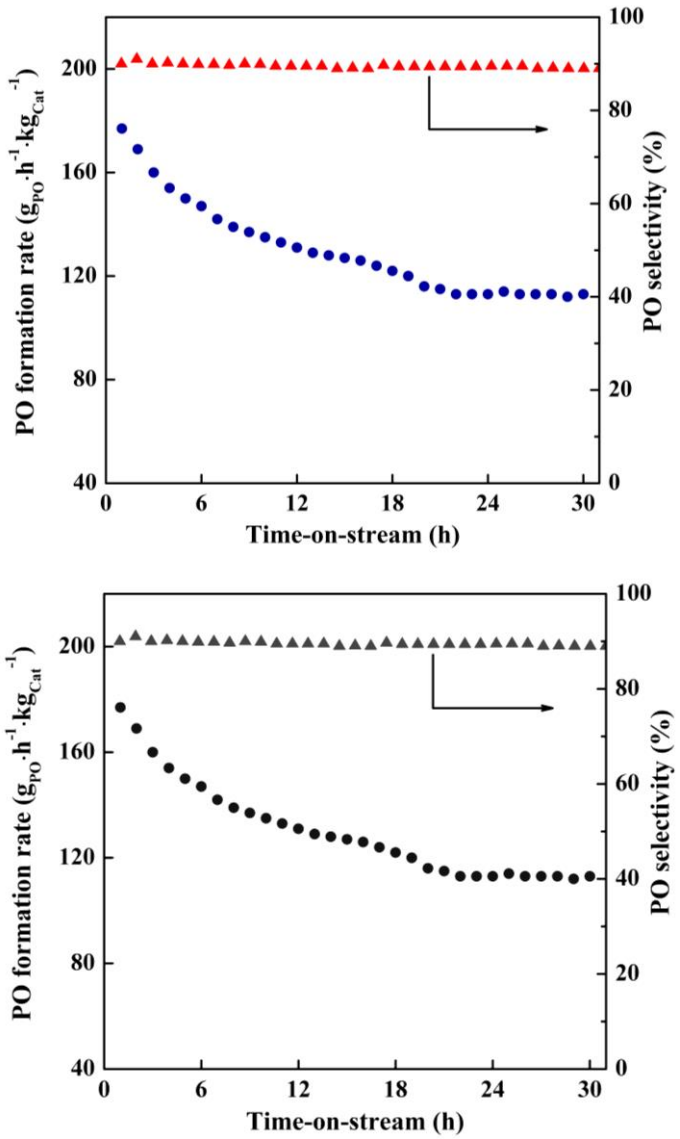

Fig. 1. PO formation rate and selectivity of 0.10 wt% Au/TS-1-O catalyst as a function of time-on-stream.

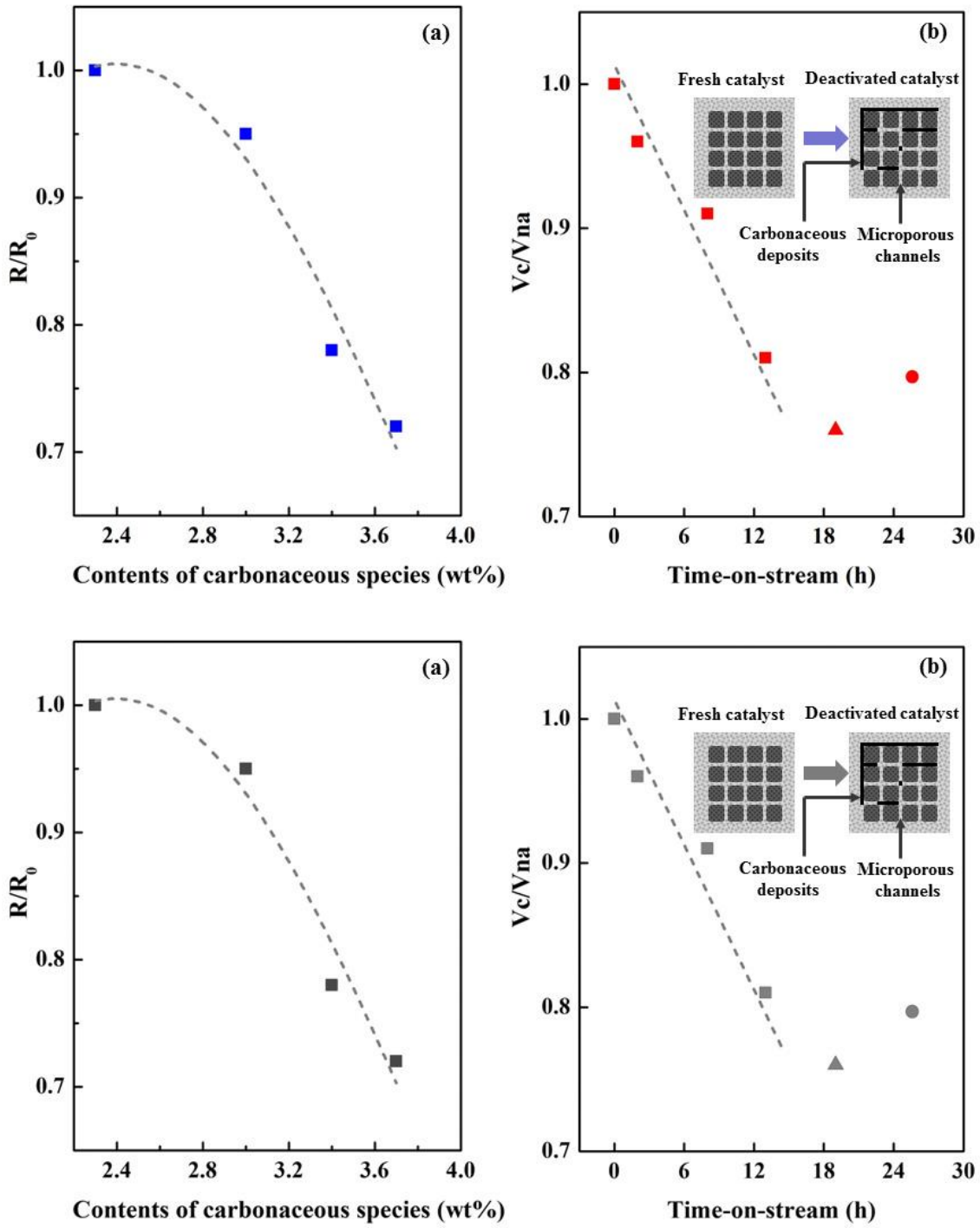

Fig. 2. (a) PO formation rate divided by the initial PO formation rate (R/R_0) as a function of content of carbonaceous deposits, and (b) V_c/V_{na} of the used 0.10 wt% Au/TS-1-O catalyst at different time-on-streams. The inset in (b) shows the possible distribution of carbonaceous deposits [30].

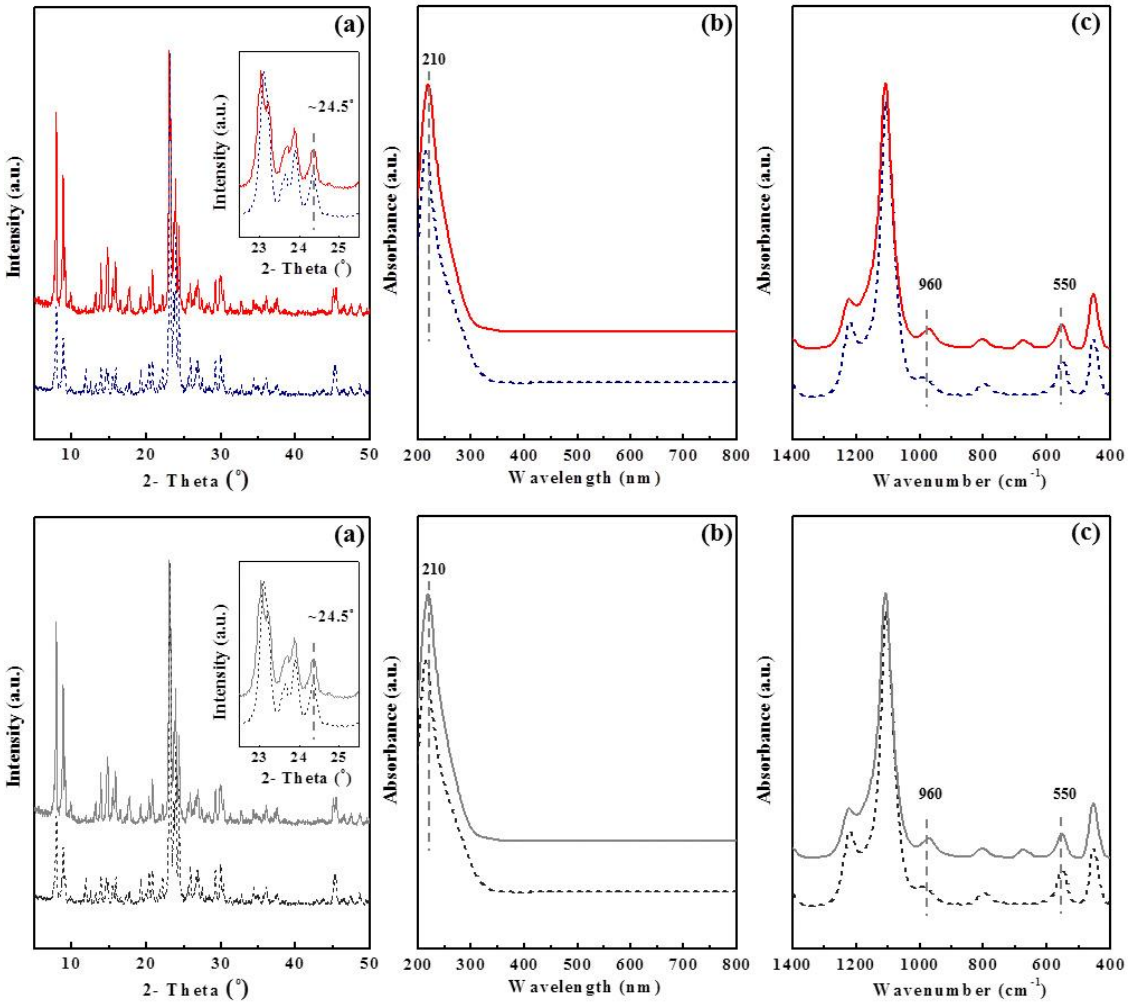

Fig. 3. (a) XRD patterns, (b) UV-vis spectra and (c) FT-IR spectra of TS-1-B (dashed line) and TS-1-O (solid line) supports.

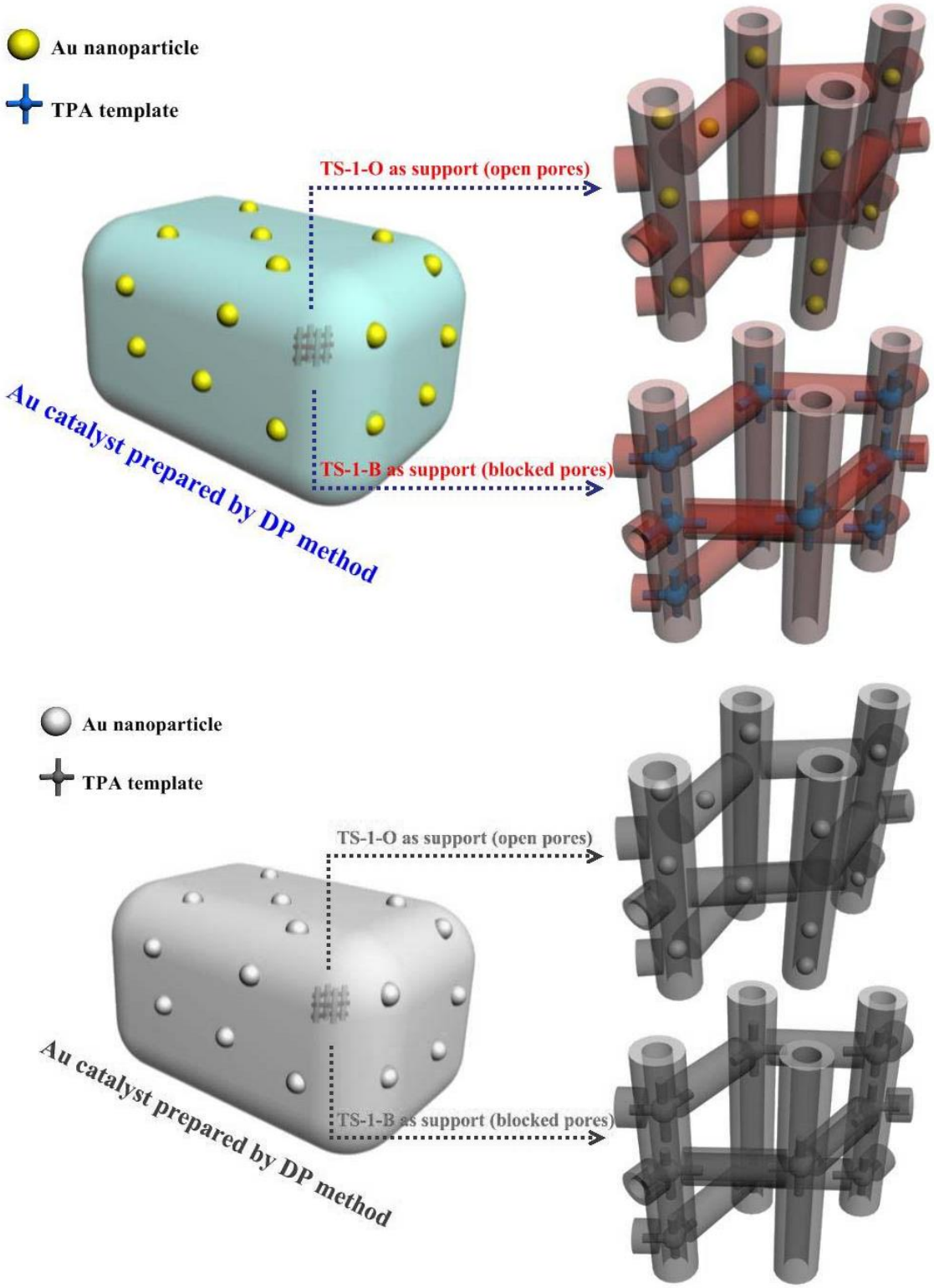

Fig. 4. Schematic diagram of Au locations of Au/TS-1-O and Au/TS-1-B catalysts.

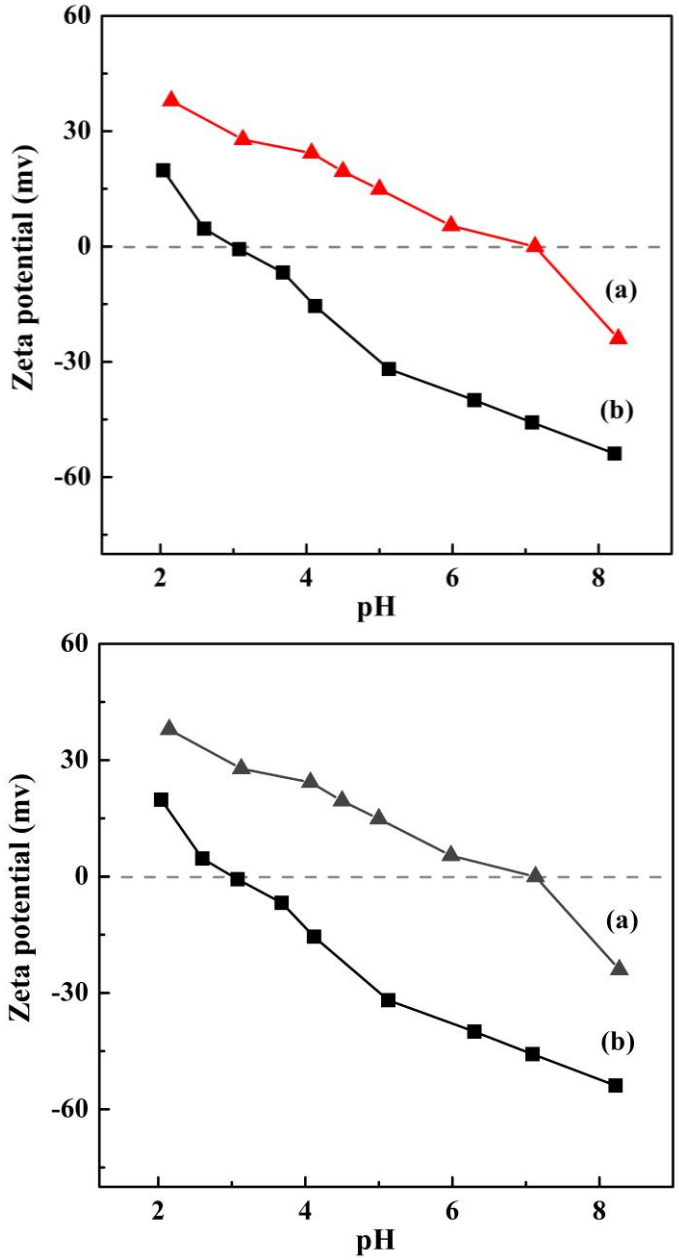

Fig. 5. Zeta potentials of TS-1-B (a) and TS-1-O (b) supports versus pH values.

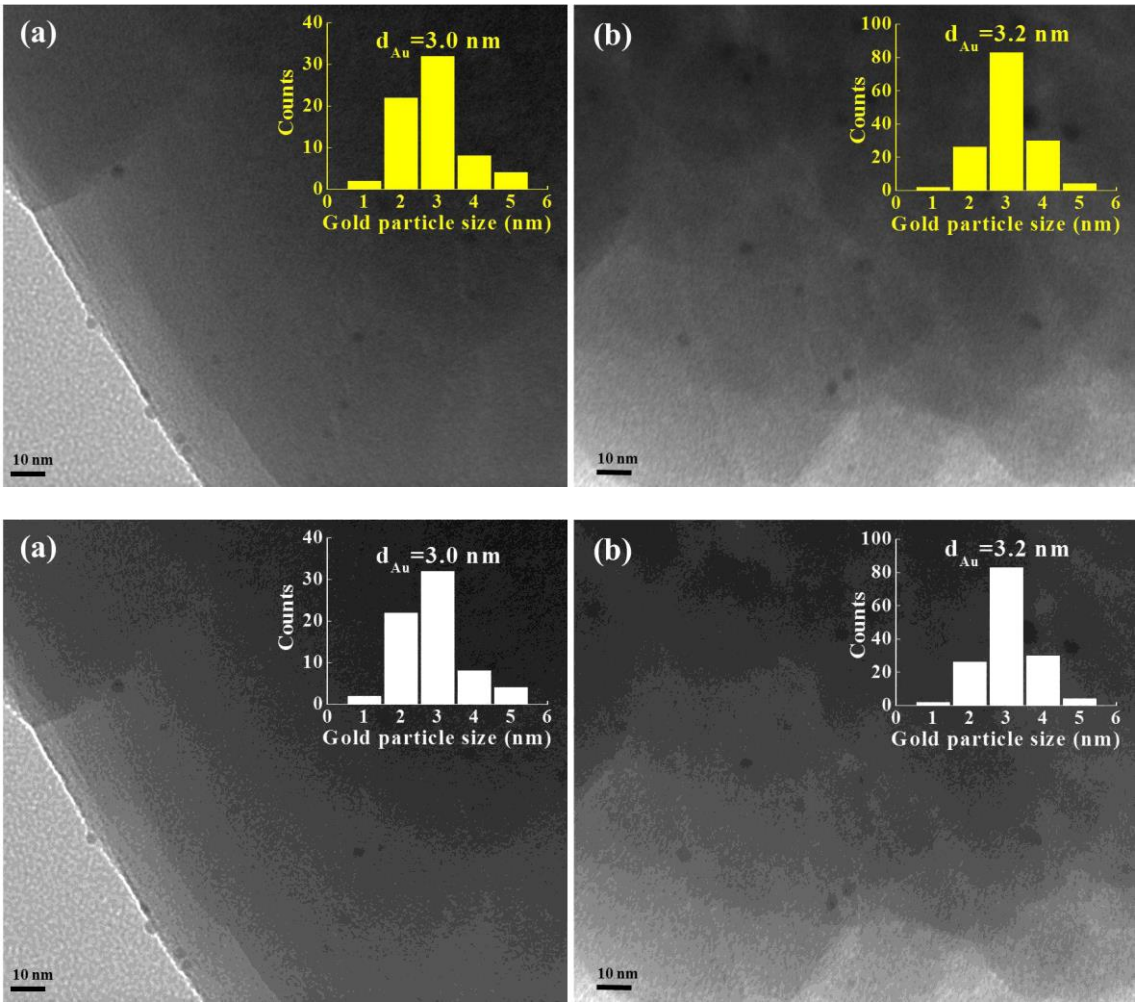

Fig. 6. Representative TEM images of the used (a) 0.10 wt% Au/TS-1-O and (b) 0.12 wt% Au/TS-1-B catalysts at 200 ^{o}C for 4 h. The insets show the particle size distributions of the two catalysts, and the scale bars represent 10 nm.

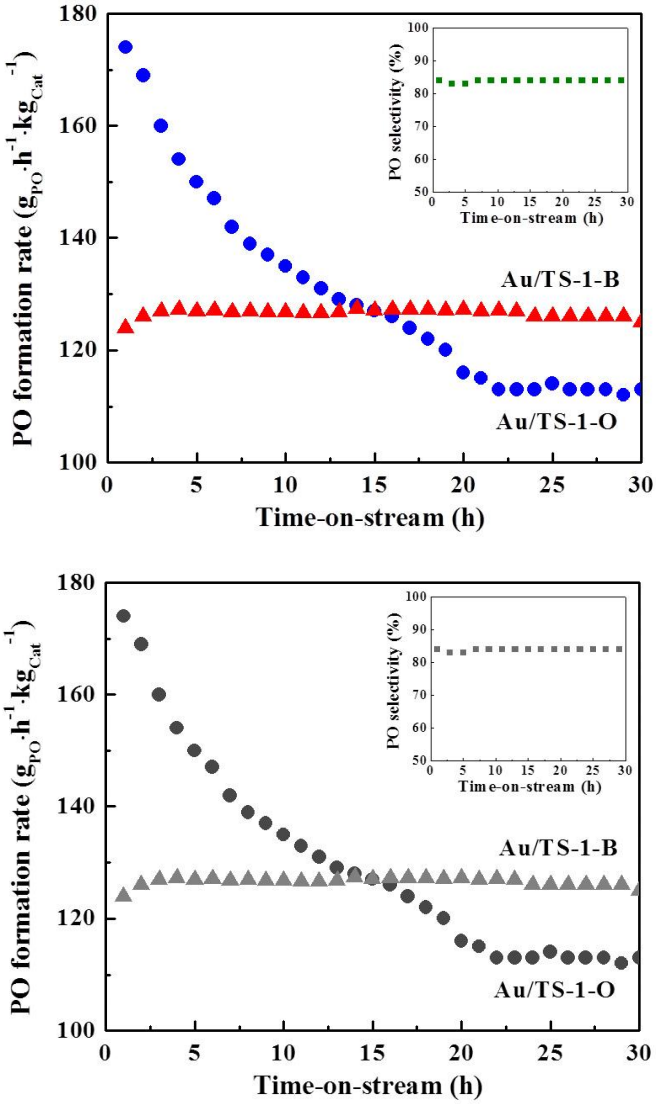

Fig. 7. PO formation rate of Au/TS-1-B and Au/TS-1-O catalysts as a function of the time-on-stream. The data of Au/TS-1-O catalyst as a function of the time-on-stream are taken from Fig. 1 and the inset shows the selectivity of Au/TS-1-B catalyst.